SYMMETRY-PRESERVING DISCRETIZATIONS FOR LAGRANGIAN GAS DYNAMICS

L.G. MARGOLIN, M.J. SHASHKOV AND M.A. TAYLOR

Los Alamos National Laboratory, Mail Stop D413, Los Alamos NM 87545, USA
E-mail contact: M.A. Taylor, mt@lanl.gov

We present numerical results for two different symmetry-preserving discretizations that have been implemented in the Lagrangian gas dynamics code MIMIC. The first discretization uses a curvilinear grid where the cell edges are represented by arcs of circles and the differential operators are treated in a compatible way. The second discretization is a modified gradient approach where components of the gradient are rotated based on the local curvature of the grid. Both schemes exactly preserve spherical, cylindrical and planar symmetry and are equivalent for problems with these symmetries.

1 Introduction

It is common practice to apply Lagrangian gas dynamics codes to solve spherical problems in cylindrical geometry on a polar grid, while discretizing the equations of motion in Cartesian coordinates. This practice has several advantages over discretizing the equations in spherical coordinates[7], but has the drawback that the usual difference operators will not exactly preserve spherical or cylindrical symmetry of the solution.

The importance of preserving spherical symmetry in Lagrangian simulations is well recognized. For example, it is critically important for the inertial confinement fusion program, which requires the numerical simulation of implosions. There small departures from spherical symmetry coupled with strong compression may be amplified by Rayleigh-Taylor instability, leading to unacceptably large errors. Uncertainty as to whether a nonsymmetric result is due to numerical errors or to physical design inhibits our understanding of the dynamics of the implosion.

This paper presents numerical results using two recent Cartesian coordinate discretizations that are capable of preserving spherical, cylindrical and planar symmetry present in the fluid flow. The first makes use of a higher order curvilinear grid[7], while the second is based on the modified gradient approach[3]. The feature we focus on here is the ability of these methods to preserve a spherically symmetric solution on a polar grid in cylindrical geometry, without requiring that the polar grid be equally spaced in angle or radius.

To study these methods, we use the two-dimensional (Cartesian or cylindrical $r - z$ geometry) Lagrangian code MIMIC (Matter In Motion Is Conservative). MIMIC solves the gas dynamics equations with energy-preserving compatible differencing[1]. It uses a conventional staggered discretization on a logically rectangular grid. The velocities are stored at the nodes, while all other quantities are at cell centers. To control the anomalous grid distortion and tangling common to Lagrangian codes, MIMIC uses a sub-zonal mass and pressure technique[2].

In what follows we present results for two model problems for three discretizations: an unmodified compatible differencing and two symmetry-preserving methods. The first problem is the Coggeshall-Meyer-ter-Vehn analytic solution[6]. This problem is not spherically symmetric, but we use it to compare accuracy and convergence rates for all three numerical methods. The second problem models a spherical Rayleigh-Taylor instability. In this highly unstable case, asymmetric truncation errors are shown to trigger the growth of an unphysical mode. Both symmetry-preserving methods avoid this problem.

2 Symmetry-preserving discretizations

The Lagrangian equations of the gas dynamics equations solved by MIMIC are

$$\rho \frac{d\mathbf{v}}{dt} = -\nabla p \tag{1}$$

$$\rho \frac{de}{dt} = -p \nabla \cdot \mathbf{v}. \tag{2}$$

MIMIC moves the grid with the velocity $\mathbf{v}$ resulting from Eq. (1) and updates the internal energy e with Eq. (2). The mass is constant within a cell, and the density ρ can be computed from the known mass and the cell volume, where the volume is computed exactly from the computational grid. The pressure p, internal energy and density are related by an equation of state.

A typical control volume for the curvilinear and unmodified differencing is shown in Fig. 1. Here we show four cells from a polar grid where we have assumed a spherically symmetric pressure p. In the compatible differencing used by MIMIC, the gradient at a node involves sums of pressure forces divided by the control volume. The pressure forces are products of the pressure, cell edge surface area and unit vectors normal to the cell edges. Two of the unit vectors normal to the cell edges are shown in the figure, denoted by $\hat{n}_L$ and $\hat{n}_R$ and normal to the cell edges denoted by S_L and S_R, respectively.

The first symmetry-preserving discretization achieves symmetry with a curvilinear grid[7] that uses higher-order curves to represent the cell edges. The

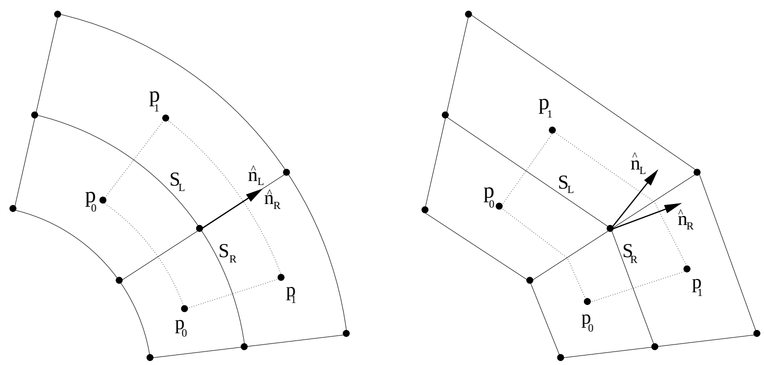

Figure 1. Control volume for curvilinear differencing (left) and unmodified differencing (right). Four cells are shown, drawn with solid lines and the control volume is drawn with dotted lines. Pressure and density are cell centered and the velocity is stored at the cell vertices.

curves are reconstructed by estimating the curvature from the position of the nodes. The curves are allowed to be straight lines or arcs of circles, and the procedure is exact for rectangular and polar grids. Using this higher-order representation of the cell edges, the cell edge normal vectors are also computed exactly for rectangular and polar grids (equally or unequally spaced), as shown in the Fig. 1. The only modification to the compatible differencing used in MIMIC is in the definitions of edge lengths, surface area and cell volumes, which are modified to give the correct values assuming curvilinear cell edges. The resulting formulas are consistent with the unmodified compatible differencing and thus retain all conservation properties.

The second symmetry-preserving discretization is the modified gradient approach[3], which modifies the direction of the normal vectors used in constructing the gradient and divergence operators. In the modified gradient approach, one first computes a higher-order estimate of the cell edge normals based on local estimates of the grid curvature. This normal is then used to construct a higher-order correction for the direction of the pressure forces. With spherically symmetric data and a polar or rectangular grid (equally or unequally spaced) the gradient will be in the radial direction with magnitude only a function of radius.

For a spherically symmetric state (that is, all variables depend only on the radius R), both the curvilinear and modified gradient discretizations give divergences which depend only on R, and gradients in the radial direction with magnitudes which only depend on R. This feature allows both methods to preserve spherical symmetry, even on polar grids that are not equally spaced in angle. Furthermore, with spherically symmetric data, the modified gradient and curvilinear discretizations give identical results, even though the two schemes have very different constructions. We describe why this is true for the gradient operator below. A similar argument holds for the divergence.

The gradient operator is a sum of components involving the ratio of surface areas to volumes. In the case of spherically symmetric data on a polar grid, any θ dependence in this ratio breaks spherical symmetry. On a polar grid, the R and θ dependence of areas and volumes is separable, and the symmetry-preserving schemes provide very different mechanisms to remove the θ dependence. The remaining term is the R dependence of the ratio of cell surface areas to the cell volume. However, this R dependence turns out to be the same whether computed assuming straight cell edges (as in the modified gradient approach) or curvilinear edges from the curvilinear symmetry-preserving method. Thus in the case of spherical symmetry, the two discretizations produce identical results.

For problems close to spherical symmetry, the two schemes will produce different results, although we have found that the differences are small and not significant. For very irregular grids far from spherical symmetry, both methods are disabled in MIMIC through the use of limiters that default to the unmodified compatible differencing.

3 Coggeshall-Meyer-ter-Vehn convergence study

Our first simulations are of the Coggeshall-Meyer-ter-Vehn model problem. It has an analytic solution allowing us to use this problem for a rigorous convergence study. This problem is a special case of a general set of solutions to the inviscid hydrodynamic equations in three dimensions[6]. It is a simple adiabatic compression problem that becomes singular at t=1.0. For our convergence study, we focus on the L_2 error at $t = 0.8$.

The exact solution is given by

$$u = \frac{-r}{1-t}, \qquad v = \frac{-z}{4(1-t)}$$

$$\rho = (1-t)^{-9/4}, \qquad e = \left(\frac{3z}{8(1-t)}\right)^2, \qquad p = \frac{2}{3}e\rho.$$

The components of the velocity in the r and z direction are given by u and v respectively. The density, pressure and internal energy are denoted ρ, p and e respectively.

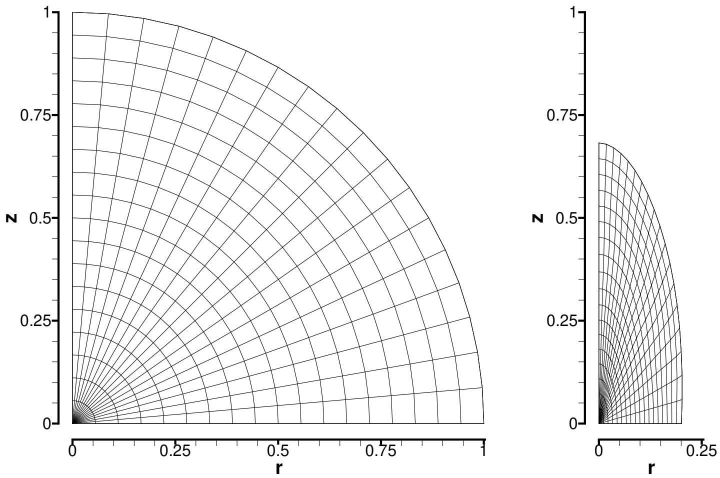

Figure 2. Computed solution of the Coggeshall-Meyer-ter-Vehn problem for t=0.0 (left) and t=0.8 (right) on a 20x20 Lagrangian grid.

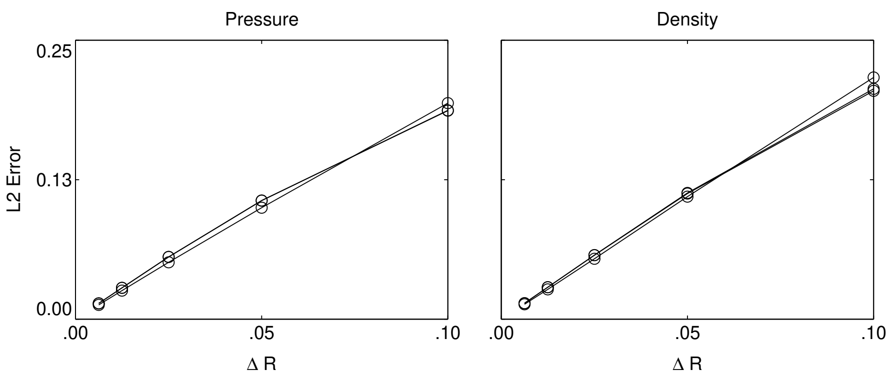

Figure 3. Convergence study for the Coggeshall-Meyer-ter-Vehn problem. The error at t=0.8 is plotted as a function of the initial radial mesh spacing ΔR.

We use the exact solution to generate the initial conditions at time $t = 0.0$. The initial grid is shown in Fig. 2. The problem is solved in cylindrical geometry, with rotation about the z axis. The boundary conditions on the r and z axes are free slip. By reflecting the solution about $z = 0$, we can consider the simulation to be modeling a collapsing sphere with cylindrical symmetry. For the outer boundary, we prescribe the pressure using the values from the analytic solution. The final state at t=0.8 of the computed solution is also shown in Fig. 2.

A convergence study was performed using all three methods, using grids up to 160x160. For this problem, which does not contain spherical symmetry but does have significant curvature of the grid lines, all the methods were for the most part indistinguishable and showed first-order convergence. This convergence is shown in Fig. 3. The errors for all three discretizations are plotted.

4 Spherical Rayleigh-Taylor instability

This problem is a spherical version of the Rayleigh-Taylor instability. Radial gravity is used, with an unstable interface placed at radius $R = 1$. The computational domain is $.25 \leq R \leq 1.75$. We use a γ-law gas with $\gamma = 1.4$. The initial velocity for all nodes is zero. The density is 100.0 for $R > 1$ and 1.0 for $R < 1$. The initial pressures are chosen to be in exact hydrostatic balance. The gravitational constant is taken as 0.02.

The first simulation uses a polar grid without any initial perturbation. The initial grid is not shown, but it is identical to the grid on the right in Fig. 4. Due to the lack of symmetry preservation in the conventional discretization, the asymmetric truncation error quickly triggers the instability, and by time $t = 6$ has produced the unphysical mode shown in Fig. 4. Both symmetry-preserving schemes do not trigger any instability. The solution at $t = 6$ is unchanged from the initial condition as shown in Fig. 4.

The second simulation uses a grid with an initial perturbation. The initial conditions are identical to the unperturbed case, except for a perturbation (not visible to the naked eye) in the grid position along $R = 1$. Let θ_i be the usual angle in the $r - z$ plane of the points along $R = 1$ in the unperturbed grid. The perturbed grid replaces these points with

$$r_i = (1 + f(\theta_i))\cos(\theta_i) \tag{3}$$

$$z_i = (1 + f(\theta_i))\sin(\theta_i) \tag{4}$$

The perturbation f is designed to give a very small indentation around the north pole. The exact form is given by

$$f = -.002\left(1 + 6.5\left(\frac{\pi}{2} - \theta_i\right)^2\right)^{-1}$$

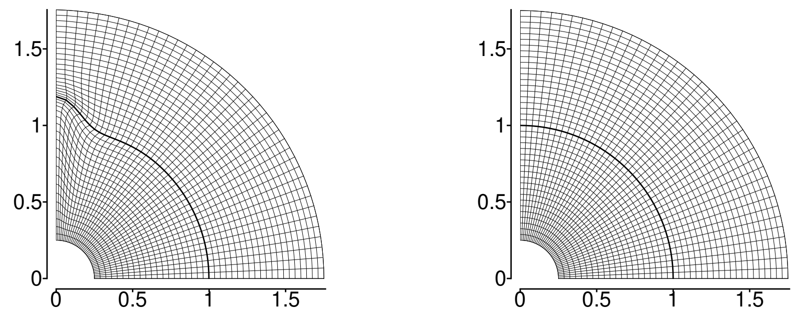

Figure 4. Spherical Rayleigh-Taylor problem at t=6.0 with no initial perturbation, solved with unmodified compatible differencing (left) and curvilinear differencing (right).

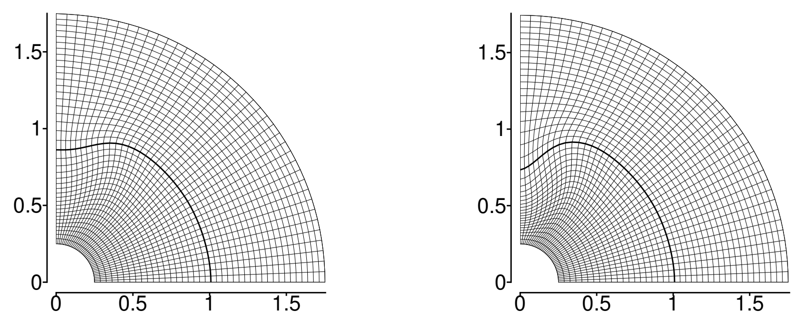

Figure 5. Spherical Rayleigh-Taylor problem at t=6.0 with an initial polar perturbation, using unmodified compatible differencing (left) and curvilinear differencing (right).

The solutions at time $t = 6$ for this case, using curvilinear differencing is shown in Fig. 5. The solution using the modified gradient method is visually identical to the curvilinear result and is not shown. Both methods exhibit the expected growth of the initial perturbation. The maximum growth rate is along the z axis, where the initial perturbation is largest.

The solution without using a symmetry-preserving scheme is shown in Fig. 5. It is visibly different than that produced by the symmetry-preserving schemes. It appears to be a linear combination of the unphysical mode triggered by the asymmetric truncation error and the more conventional mode exhibited by the symmetry preserving schemes. With unmodified differencing, the maximum growth rate is no longer along the z axis, even though the initial perturbation is largest at the z axis.

5 Conclusions

We have compared a standard Lagrangian hydrodynamic scheme based on compatible differencing with two alternate schemes modified to better preserve spherical symmetry. We have found that the two modified schemes do not decrease accuracy in problems where spherical symmetry is not expected. However the modified schemes do improve accuracy in spherically symmetry problems, especially in representing the effects of unstable perturbations.

We also note that the two modified schemes, which are based on different constructions, give essentially identical results for a variety of initial meshes that reflect the expected spherical symmetry. This is a result of the separability of fundamental operators divergence and gradient when written as functions of radius and angle. This equivalence suggests that mesh itself is not of direct importance, but merely helps to implement more fundamental relations that act to preserve symmetry.

We note that both the curvilinear grid approach[5] and the modified gradient approach[4] have been extended to fully three-dimensional algorithms.

We gratefully acknowledge the support of the Department of Energy's Accelerated Strategic Computing Initiative, and of the Los Alamos National Laboratory's Directed Research and Development program. This work has benefited greatly from detailed discussions with J.C. Campbell, E.J. Caramana, and T.L. Wilson.

References

1. E.J. Caramana *et al*, *J. Comp. Phys.* **146**, 227 (1999).
2. E.J. Caramana and M.J. Shashkov, *J. Comp. Phys.* **142**, 521 (1999).
3. E.J. Caramana and P.P. Whalen, *J. Comp. Phys.* **141**, 174 (1998).
4. E.J. Caramana, C.L. Rousculp and D.E. Burton, submitted *J. Comp. Phys.*
5. R. Liska, M.J. Shashkov and B. Swartz, submitted *Comput. Aided Geom. Des.*
6. S.V. Cogeshall and J. Meyer-ter-Vehn, *J. Math. Phys.* **33**, 3585 (1992).
7. L.G. Margolin and M.J Shashkov, *J. Comp. Phys.* **149**, 389 (1999).